Journal of Remote Sensing
A SCIENCE PARTNER JOURNAL

RESEARCH ARTICLE

Absorption Coefficient and Chlorophyll Concentration of Oceanic Waters Estimated from Band Difference of Satellite-Measured Remote Sensing Reflectance

Zhongping Lee[1*], Longteng Zhao[1], Chuanmin Hu[2], Daosheng Wang[1], Junfang Lin[3], and Shaoling Shang[1]

[1]State Key Laboratory of Marine Environmental Science, College of Ocean and Earth Sciences, Xiamen University, Xiamen 361102, China. [2]College of Marine Science, University of South Florida, St. Petersburg, St. Petersburg, FL 33701, USA. [3]Plymouth Marine Laboratory Prospect Place, The Hoe, Plymouth PL1 3DH, UK.

*Address correspondence to: zhongping.lee@umb.edu

Citation: Lee Z, Zhao L, Hu C, Wang D, Lin J, Shang S. Absorption Coefficient and Chlorophyll Concentration of Oceanic Waters Estimated from Band Difference of Satellite Measured Remote Sensing Reflectance. *J. Remote Sens.* 2023;3:Article 0063. https://doi.org/10.34133/remotesensing.0063

Submitted 15 April 2023
Accepted 29 June 2023
Published 27 July 2023

Absorption coefficient and chlorophyll concentration (*Chl*) are important optical and biological properties of the aquatic environment, which can be estimated from the spectrum of water color, commonly measured by the remote sensing reflectance (R_{rs}). In this study, we extended the band-difference scheme for *Chl* of oceanic waters developed a decade ago to the estimation of absorption coefficient at 440 nm (*a*(440)). As demonstrated earlier for the estimation of *Chl*, *a*(440) product from the band difference of R_{rs} showed much smoother spatial pattern than that from a semianalytical algorithm. More importantly, it is found that the upper limit of using band difference of R_{rs} can be extended from −0.0005 sr^{-1} (the upper limit set a decade ago for the estimation of *Chl*) to ~0.0005 sr^{-1} (corresponding to *a*(440) ~0.08 m^{-1}), which covers ~91% of the global ocean. We further converted *a*(440) to *Chl* based on the "Case-1" water assumption and found that the standard *Chl* product of oligotrophic waters (*Chl* ~ 0.1 mg/m^3) distributed by NASA is generally ~20% higher than *Chl* converted from *a*(440), possibly a result of different datasets used to determine the algorithm coefficients. These results not only extended the application of the band-difference scheme for more oceanic waters but also highlighted the need of more accurate field measurements of *Chl* and R_{rs} in oligotrophic oceans in order to minimize the discrepancies observed in satellite *Chl* products derived using the same algorithm concept but different empirical approaches.

Introduction

The absorption coefficient of aquatic environments is one of the most important environmental properties. It not only plays a key role in determining the appearance of water/ocean color [1] but also is a key property in regulating the attenuation of solar radiation through the water column from water surface [2,3], heating of the water column [4], as well as converting inorganic carbon to organic materials by phytoplankton through photosynthesis [5]. In addition, the estimation of chlorophyll concentration (*Chl*, in mg/m^3) in the surface layer via ocean color remote sensing is also through the relationship, directly or indirectly, between the absorption coefficient and chlorophyll concentration [6,7]. It is thus no surprising to see that the inversion of absorption coefficient and other inherent optical properties (IOPs) from water color is an important aspect of ocean optics and ocean color remote sensing.

In the past decades, empirical and semianalytical algorithms have been developed for the estimation of absorption coefficient (in the visible domain) from remote sensing reflectance (R_{rs}, in sr^{-1}), which is the ratio of water-leaving radiance to downwelling irradiance just above the surface [8]. These algorithms in general performed very well for error-free R_{rs}. However, as highlighted by Hu et al. [9,10], due to issues related to sensor's sensitivity, calibration to atmosphere correction, R_{rs} from ocean color satellites always contains various levels of uncertainties or errors. In particular, R_{rs} around 550 nm (R_{rs}(55x)) of oceanic waters is very small, thus containing relatively large uncertainties from those processes. Because R_{rs}(55x) of oceanic waters plays a key role in the algorithms based on the blue–green ratio of R_{rs} (represented as BGR_{Rrs} in the following) [1,11] or in the semianalytical algorithms (e.g., the quasi-analytical algorithm [QAA] and the generalized inherent optical properties [GIOP]) [12,13], these uncertainties are propagated into the estimated *Chl* or IOPs. Such uncertainties can be visualized in the *Chl* or IOP imagery speckle or pepper noises. In realizing the spectrally covarying nature of the uncertainties (errors) in satellite produced R_{rs} (due mainly to the imperfect atmospheric correction or other corrections), Hu et al. [9] proposed an innovative algorithm for the estimation of *Chl* for oceanic waters, which uses a 3-band or multi-band difference of R_{rs} (represented as MBD_{Rrs} in the following) to minimize the impact of spectrally covarying uncertainties in these bands, which substantially improved *Chl* image products in terms of reduced speckle noise and improved accuracy and cross-sensor consistency. After extensive evaluations, National Aeronautics and Space Administration (NASA), National Oceanic and Atmospheric Administration, and European Space Agency adopted this approach for the generation of *Chl* products for the various ocean color missions for *Chl* less than ~0.2 mg/m^3. Similarly, based on the same concept of band difference to minimize the impact of spectrally covarying errors from atmospheric correction, new band-difference algorithms have been proposed for the estimation of particulate inorganic carbon [14] and particulate organic carbon [15].

Here, using SeaWiFS data as an example, we extend this concept for the generation of absorption coefficient at 440 nm ($a(440)$, in m^{-1}) of oceanic waters from the error-bearing R_{rs}, in view of that the peak absorption by chlorophyll is centered at this band. Further, the estimated $a(440)$ is converted to *Chl* following the "Case-1" concept of oceanic waters. More importantly, in addition to the smoother image product of $a(440)$ from SeaWiFS by such a scheme, it appears that the upper limit of the $a(440)$-derived *Chl* could be extended to ~0.8 mg/m^3, which would then significantly expand the global applicability of *Chl* product from the band difference approach, a scheme that is much more tolerant to noises in the R_{rs} product.

Materials and Methods

Following Hu et al. [9] and for the SeaWiFS bands, the absorption coefficient at 440 nm, $a(440)$, is expressed as

$$MBD_{Rrs440} = R_{rs}(555) - \left[R_{rs}(443) + \frac{555-443}{670-443}\left(R_{rs}(670) - R_{rs}(443)\right)\right] \quad (1A)$$

$$a(440) = F\left(MBD_{Rrs440}\right) \quad (1B)$$

Here, MBD_{Rrs440} is the multiband difference of R_{rs} aimed for $a(440)$, which is the same formulation as the color index defined by Hu et al. [9] but used for a different purpose. F represents a function of MBD_{Rrs440}, which is determined by the nature and characteristics between MBD_{Rrs440} and $a(440)$. Note that due to the small difference between $a(443)$ and $a(440)$, $a(440)$ in this study represents values of absorption coefficient at 440 or 443 nm.

For an empirical algorithm represented by Eq. 1 to work well, as all empirical algorithms, a high-quality and inclusive dataset is the key. To meet this requirement, the dataset having concurrent measurements of the diffuse attenuation coefficient (K_d) and R_{rs} compiled by Lin et al. [16] were utilized, where absorption coefficients were further analytically derived from the combination of K_d and R_{rs}. Compared to the absorption coefficients determined from water samples or from hyperspectral absorption and attenuation meters (WET Labs Inc., USA), the derived absorption coefficients from K_d and R_{rs} have much higher fidelity [16]. Further, this IOP dataset was augmented with measurements from the Biogeochemistry and Optics South Pacific Experiment (BIOSOPE) cruise [17], which was taken in the South Pacific Gyre covering the clearest natural waters. While the Lin dataset covered oceanic to coastal waters, the addition of BIOSOPE data is critical for the MBD_{Rrs}-based algorithm as such a scheme works the best for oligotrophic waters. For consistency with the Lin dataset, the absorption coefficients of the BIOSOPE dataset were also derived from a combination of the diffuse attenuation coefficient (K_d) and R_{rs} following the approach described by Lin et al. [16]. Figure 1 shows the distributions of $a(440)$ of this dataset (termed as $a(440)_{Kd}$), where $a(440)_{Kd}$ varied in a range of ~0.01 to 2.0 m^{-1}. There are nearly 700 points having $a(440)_{Kd}$ < 0.1 m^{-1}, corresponding to *Chl* ~1.0 mg/m^3 following Morel and Maritorena [18].

To check the quality of this dataset, the total absorption coefficient was further inverted from R_{rs} following QAA (termed as $a(440)_{QAA}$) [12], with Fig. 2 showing a comparison of $a(440)$ from the two independent determinations. For the wide range of $a(440)$, the coefficient of determination (R^2) is 0.98 (N = 1,161), with a slope as 0.96, negligible intercept, and an average of unbiased absolute relative difference of 12.8%. These measures suggest that this $R_{rs}(\lambda)$ and $a(440)$ matchup dataset has an excellent fidelity.

Results and Discussion

A) Empirical algorithm for the absorption coefficient

Figure 3 shows the relationship between MBD_{Rrs440} and $a(440)_{Kd}$&$a(440)_{QAA}$. It is found that for MBD_{Rrs440} < ~0.0005 sr^{-1}, a tight dependence emerged between MBD_{Rrs440} and $a(440)$. This upper limit of 0.0005 sr^{-1} is a significant extension of that determined by Hu et al. [9] for the estimation of *Chl*, where the upper limit was set as −0.0005 sr^{-1}. The extension, at least for this dataset, indicates that band difference of R_{rs} could be applied for much wider range of waters.

Further, Fig. 3 suggests that $\log(a(440))$ varies nonlinearly with MBD_{Rrs440}; we thus used the following formula to empirically estimate $a(440)$ from MBD_{Rrs440},

$$a(440) = 10^{-2.21+1.01\ \mathrm{Exp}\left(228.82\times MBD_{Rrs440}\right)} \quad (2)$$

The model coefficients (for SeaWiFS bands), −2.21, 1.01, and 228.82, were obtained through least-square fitting against $a(440)_{QAA}$ for MBD_{Rrs440} up to 0.0005 sr^{-1}, as $a(440)_{QAA}$ representing an average dependence between $a(440)$ and MBD_{Rrs440} for this dataset. Figure 4 compares Eq. 2 modeled $a(440)$ (termed as $a(440)_{MBD}$) vs known $a(440)$, where there is an excellent agreement for $a(440)$ up to ~0.08 m^{-1}. For $a(440)_{MBD}$ < 0.08 m^{-1}, the mean unbiased absolute relative difference (MUARD) is 4.6% between $a(440)_{MBD}$ and $a(440)_{QAA}$, with R^2 as 0.98; or MUARD

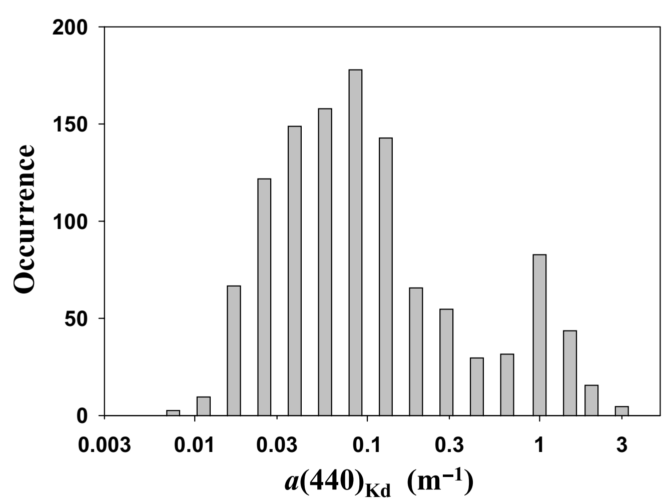

Fig. 1. Range and distribution of $a(440)$ used in this study.

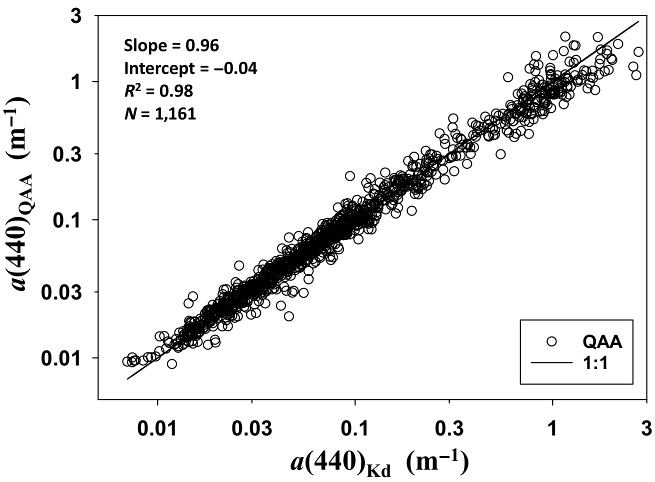

Fig. 2. Comparison between $a(440)_{Kd}$ and $a(440)_{QAA}$ of datasets used in this study.

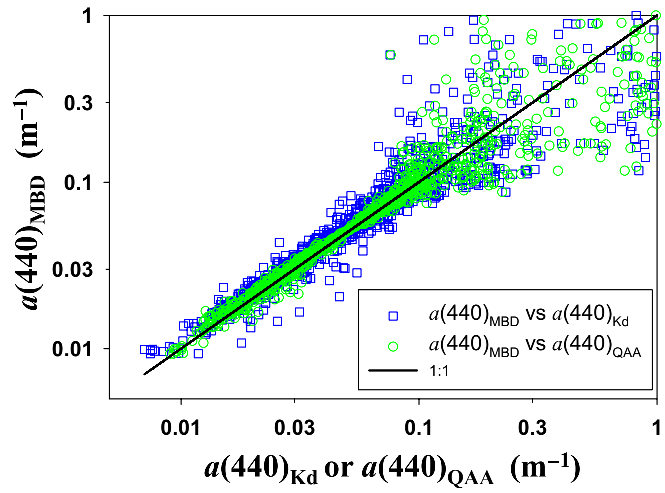

Fig. 4. Equation 2 estimated $a(440)$ is compared with known $a(440)$.

as 11.0% and R^2 as 0.90 between $a(440)_{MBD}$ and $a(440)_{Kd}$. These statistical measures indicate a robust relationship between $a(440)$ and MBD_{Rrs440} for these oceanic waters. Here, MUARD is calculated as following,

$$\text{MUARD} = \frac{2}{N}\sum_{1}^{N}\frac{|x_i - y_i|}{x_i + y_i} \quad (3)$$

with x_i and y_i representing the two independent sets of $a(440)$ under evaluation.

The band-difference algorithm is suitable only for oligotrophic waters, where the upper limit of MBD_{Rrs440} was set as -0.0005 sr^{-1} for the estimation of *Chl* in the study by Hu et al. [9], corresponding to *Chl* ~0.25 mg m^{-3}. In order to determine a suitable upper limit of MBD_{Rrs440} for the estimation of $a(440)$, Table 1 lists the performance of the MBD_{Rrs440} inversion method, with MBD_{Rrs440} being under 0.001, 0.0005, and 0 sr^{-1}, respectively. With the decrease of MBD_{Rrs440} among the 3 limits, the R^2 values increased from 0.95 to 0.99, while slope decreased from 1.04 to 1.0, all with negligible intercepts. These comparisons suggest that for waters with MBD_{Rrs440} > ~0.0005 sr^{-1}

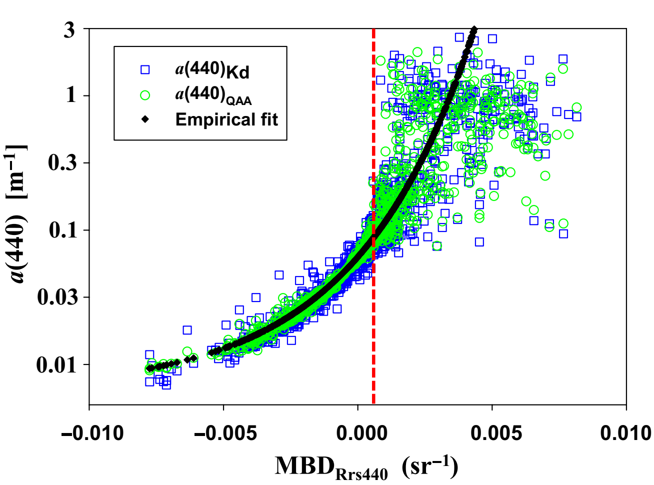

Fig. 3. Relationship between $a(440)$ and MBD_{Rrs440}. The red vertical line indicates the location of MBD_{Rrs440} = 0.0005 sr^{-1}.

($a(440)$ > ~0.084 m^{-1}), the impact of particle backscattering is getting stronger [9]; thus, there are higher uncertainties in the estimated $a(440)$ from MBD_{Rrs440} (also see Fig. 3). Compared to those with MBD_{Rrs440} < 0.0005 sr^{-1}, the agreement between $a(440)_{MBD}$ and known $a(440)$ (either $a(440)_{Kd}$ or $a(440)_{QAA}$) is slightly stronger for MBD_{Rrs440} < 0 sr^{-1} ($a(440)_{MBD}$ < ~0.063 m^{-1}), but the difference is small. In view of this small difference in performance, and with a goal to obtain more coverage with such an innovative multiband-difference algorithm, we tentatively set the upper limit of MBD_{Rrs440} as 0.0005 sr^{-1}, corresponding to $a(440)$ as 0.084 m^{-1} following Eq. 2. Spatially, this upper limit extended the coverage of the MBD_{Rrs} scheme from ~73% of the global ocean (−0.0005 sr^{-1} as the limit) to ~91%, which is a significant expansion of the MBD_{Rrs} approach for processing global ocean color satellite data.

B) Application to SeaWiFS images and its comparison with semi-analytical algorithm

To demonstrate the applicability of MBD_{Rrs} for the absorption coefficient, we applied Eq. 2 to a randomly selected SeaWiFS image, which was collected on June 9, 2008, with Fig. 5 showing the spatial distribution of the obtained $a(440)_{MBD}$. Also included in Fig. 5 is the $a(440)$ product distributed by NASA (represented as $a(440)_{GIOP}$), which was obtained from the GIOP algorithm [13], an approach completely independent of the MBD_{Rrs} algorithm for $a(440)$. Figure 6 shows scatterplots between $a(440)_{MBD}$ and $a(440)_{GIOP}$ for this SeaWiFS measurement. It is found that the two independent determinations of $a(440)$ are highly consistent, with R^2 ~ 0.91, slope close to 1.0, negligible intercept, and MUARD as ~9.6%. These results provide an independent verification of $a(440)_{MBD}$ for oceanic waters in the general patterns of spatial distributions.

On the other hand, it is clear that there are deviations of $a(440)_{GIOP}$ for a given $a(440)_{MBD}$ (see Fig. 6). This deviation, in part due to different strategies of algorithms, also reflects the impact of noises in R_{rs} spectrum that were propagated to the retrieved $a(440)_{GIOP}$. This impact can be demonstrated with the coefficient of variation of $a(440)$ (represented as $CV_{a(440)}$) for any box with 3 × 3 pixels and having at least 5 valid satellite products. Figure 7 shows the histogram of $CV_{a(440)}$ for $a(440)_{MBD}$ in the range of 0.02 to 0.04 m^{-1}, reflecting clear oceanic waters

Table 1. Statistics between $a(440)_{MBD}$ and known $a(440)$ ($a(440)_{QAA}$ and $a(440)_{Kd}$, respectively) under different upper limits of MBD_{Rrs440}.

	Upper limit of MBD_{Rrs440} (sr^{-1})	R^2	Slope	Intercept	MUARD	N
$a(440)_{MBD}$ vs $a(440)_{QAA}$	0.001	0.95	0.91	0.0036	0.054	773
	0.0005	0.98	0.96	0.0016	0.046	668
	0	0.99	0.98	0.0007	0.045	547
$a(440)_{MBD}$ vs $a(440)_{Kd}$	0.001	0.89	0.87	0.0065	0.116	773
	0.0005	0.89	0.88	0.0055	0.111	668
	0	0.89	0.89	0.0044	0.108	547

where the spatial variation of physical-biogeochemical properties is in general mild. For $a(440)_{MBD}$, the range of $CV_{a(440)}$ is 0.01 to 0.12, with a mode as 0.025; however, for $a(440)_{GIOP}$, the range of $CV_{a(440)}$ is 0.01 to 0.20, with a mode as 0.038. These results further indicate the better tolerance of MBD to the noises in measured R_{rs} spectra.

C) Estimation of oceanic *Chl* from *a*(440)

There could be multiple applications of the estimated total absorption coefficient, for example, estimating *Chl* from $a(440)$. Based on broad coverage of in situ measurements, Morel and Maritorena [18] showed that the apparent optical properties [19] of oceanic waters to the first order can be modeled as a function of *Chl*, which is the base of band ratio of R_{rs} to estimate *Chl* [1,18]. This is also the commonly termed "Case-1" system [20–22]. Thus, following the steps (Eqs. 3 to 5 and 8 – 8") articulated by Morel and Maritorena [18], the K_d spectrum of a given *Chl* can be converted to the spectrum of total absorption coefficient. Subsequently, a relationship (see Eq. 4 and Fig. 8) between *Chl* and $a(440)$ can be developed for global oceanic waters under the "Case-1" assumption, expressed as (here *Chl* is limited to a range of 0.01 to 2.0 mg/m^3)

$$a(440) = 0.0044 + 0.093\, Chl^{0.654} \tag{4}$$

where 0.0044 m^{-1} is the absorption coefficient of pure seawater at 440 nm [23]. This dependence is supported by modeling $a(440)$ as a sum of three general constituents [24]

$$a(440) = a_w(440) + a_p(440) + a_y(440) \tag{5A}$$

$$= a_w(440) + A(440)Chl^{B(440)}\,[1 + Y] \tag{5B}$$

with subscripts "w, p, y" representing pure seawater, particles, and yellow substance, respectively. Values of A and B are available from Bricaud et al. [25]. Considering the absorption coefficient of yellow substance covaries with that of phytoplankton for "Case-1" waters [20,21] and taking a Y value as 0.8 [26,27], the relationship between $a(440)$ and *Chl* following Eq. 5 is also included in Fig. 8. For *Chl* in a range of 0.01 to 2.0 mg/m^3, $a(440)$ values resulted from the two completely independent approaches (Eqs. 4 and 5) are nearly identical, with MUARD as 2.3% and R^2 ~ 1.0. These results indicate a solid general relationship between *Chl* and $a(440)$ for such "Case-1" waters.

Thus, when $a(440)$ is obtained by Eq. 2, *Chl* can be further estimated following Eq. 4, with results termed as Chl_{a440}. We compared Chl_{a440} with *Chl* from water samples of two datasets (see Fig. 9): the NASA bio-Optical Marine Algorithm Dataset (NOMAD) [28] and the satellite-in situ datasets compiled by Hu et al. [9]. As *Chl* estimated from $a(440)$ covers values higher than 0.25 mg/m^3, for reference, the performance of BGR_{Rrs} (OC4) algorithm for *Chl* [11] (results termed as Chl_{OC4}) with the same datasets was also included for comparison. The statistical measures (see Table 2) of the two approaches show

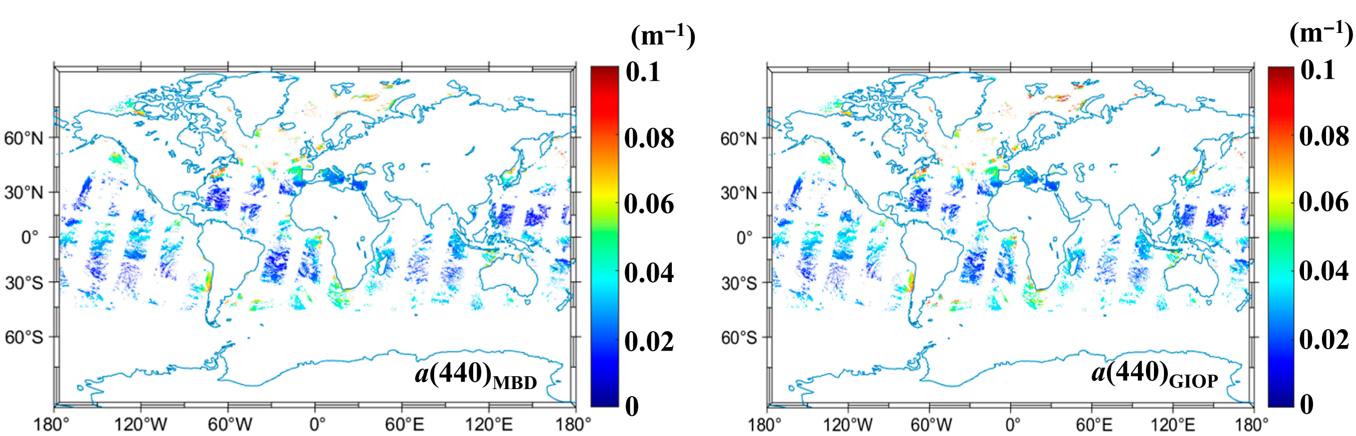

Fig. 5. Global distribution of $a(440)$ obtained from either MBD_{Rrs} (for MBD_{Rrs440} < 0.0005 sr^{-1}) or GIOP for SeaWiFS measurements of June 9, 2008. White color for land or no valid retrievals.

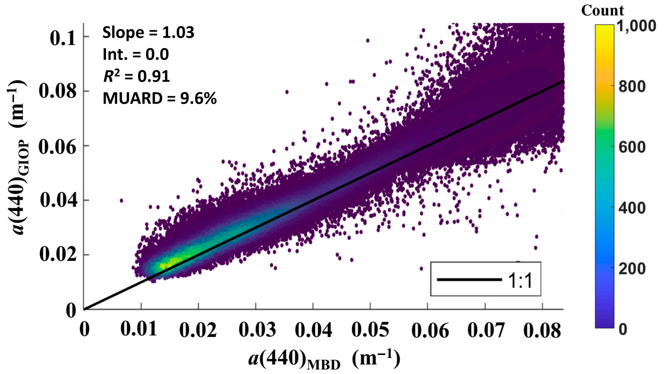

Fig. 6. Comparison between $a(440)_{MBD}$ and $a(440)_{GIOP}$ for valid data in Fig. 5.

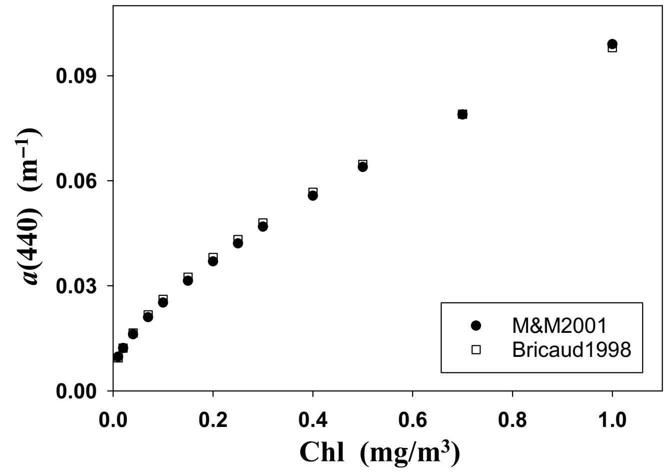

Fig. 8. Relationship between $a(440)$ and *Chl* for oceanic waters under the "Case-1" assumption.

slightly different results from that of Table 1 by Hu et al. [9] because (a) fluorometric *Chl* is used here and (b) the data covers a much wider range. Overall, these statistical measures are very similar, with OC4 showing slightly higher R^2 and lower root mean square difference (RMSD) for NOMAD. However, it is necessary to keep in mind that the algorithm coefficients of OC4 were optimized with NOMAD, but the algorithm coefficients of MBD_{Rrs} were independent of NOMAD. These results thus indicate that for waters with MBD_{Rrs440} up to 0.0005 sr^{-1}, there are no preference between the 2-step (MBD_{Rrs}-$a(440)$) and 1-step (OC4) schemes on the estimation of *Chl* from R_{rs}. The same observations are obtained from the SeaWiFS-in situ dataset. These results suggest that when being evaluated with discrete data points, at least for data used in this study, the performance of both OC4 and MBD_{Rrs}-$a(440)$ schemes in estimating *Chl* is similar.

However, when being evaluated using image pixels, there are noticeable differences between the two. The MBD_{Rrs}-$a(440)$ scheme (Eqs. 1 to 2 and 4) was applied to a SeaWiFS image of November 14, 2010 (randomly selected) to estimate *Chl* for MBD_{Rrs440} as high as 0.0005 sr^{-1} (corresponding to *Chl* ~0.8 mg/m^3). Figure 10 compares Chl_{a440} with the "standard" *Chl* distributed by NASA (Chl_{NASA}) that was estimated using both band difference (for *Chl* < ~0.25 mg/m^3) and band ratio (for *Chl* > ~0.25 mg/m^3) of R_{rs} [9]. It is found that for Chl_{a440} in a range of ~0.01 to 0.8 mg/m^3, the two *Chl* products are highly consistent, with MUARD as 14.8% and R^2 = 0.96 (in linear scale). For Chl_{a440} higher than ~0.2 mg/m^3, it appears that the mode of Chl_{NASA} matches that of Chl_{a440} very well for any given Chl_{a440}, except that on average Chl_{NASA} is about ~18% lower than Chl_{a440} for Chl_{a440} in the range of ~0.7 to 0.8 mg/m^3. As expected, there are obvious scatters for a given Chl_{a440}, or vice versa, indicating impacts of algorithm strategies and/or noises in R_{rs}.

Further, Chl_{NASA} is found in general higher by ~20% for Chl_{a440} around 0.1 mg/m^3, which is quite surprising as both Chl_{a440} and Chl_{NASA} were derived from MBD_{Rrs440} for *Chl* in this range. This 20% higher estimates are also observed in other randomly selected SeaWiFS images and appear consistent with an evaluation using the NOMAD dataset (after limiting MBD_{Rrs440} < −0.0005 sr^{-1} and *Chl* < 0.15 mg/m^3), where Chl_{a440}/Chl_{insitu} centered around 1.0, while Chl_{NASA}/Chl_{insitu} centered around 1.2 (see Fig. 11). The reason for this difference might be in the number and measurement methods used for the development of the two algorithms, where the regression parameters of the 1-step MBD_{Rrs} algorithm were obtained from 50 points [9], with field *Chl* measured via high-performance liquid chromatography. The *Chl*-$K_d(440)$ relationship, which is the base of the *Chl*-$a(440)$ relationship (Eq. 4), on the other hand, was based on hundreds of measurements [18], along with field *Chl* values determined fluorometrically. Although at this point we lack sufficient field measurements in such oligotrophic waters to determine the *Chl* from which algorithm is more accurate, it is necessary to note that the size of oceanic gyres is commonly based on a criterion of *Chl* as 0.07 or 0.1 mg/m^3 [29,30]. Thus, the difference between Chl_{a440} and Chl_{NASA} suggests that the size of oceanic gyres will be ~25% larger if the size is based Chl_{a440}.

For studies of global oceanic waters, it is always necessary to merge data from different ocean color satellites [31], where cross-sensor consistency is important for such merges. Hu et al. [9] showed that there is a much better consistency between SeaWiFS and MODIS *Chl* products obtained from MBD_{Rrs}, with an upper limit of MBD_{Rrs440} as −0.0005 sr^{-1} (see Fig. 20 of the study by Hu et al. [9]). Also for data of November 2006,

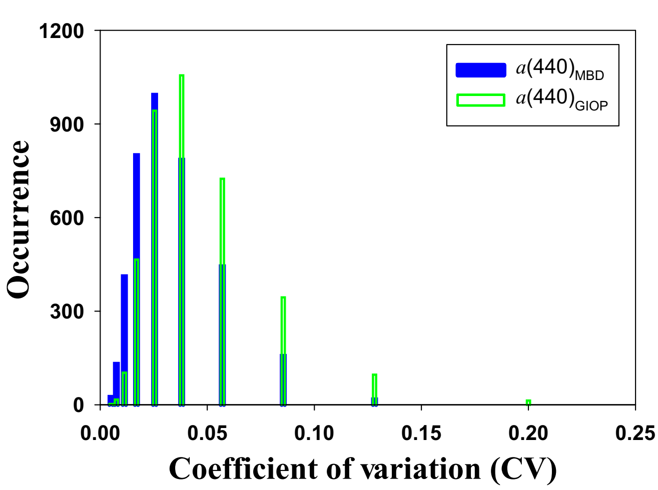

Fig. 7. Distribution of coefficient of variation (CV) of $a(440)_{MBD}$ and $a(440)_{GIOP}$, respectively, calculated for boxes with 3 × 3 pixels. The range of $a(440)_{MBD}$ is limited to 0.02 to 0.04 m^{-1}, where the spatial variation of oceanic waters is mild.

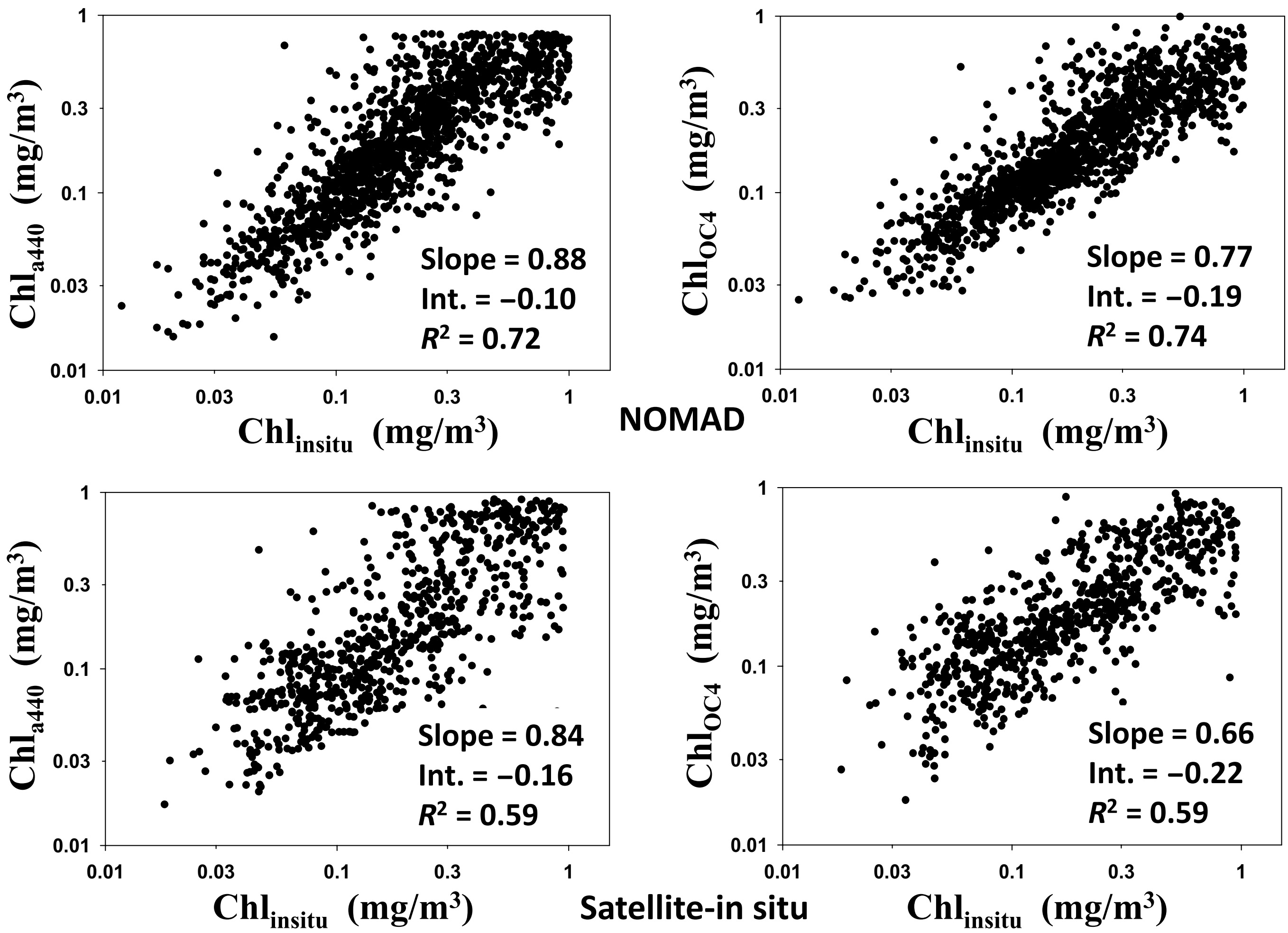

Fig. 9. Comparison between Chl_{a440}, Chl_{OC4}, and measured *Chl*, along with statistical measures (in log10 scale) included in the figures. The top panel is for the NOMAD dataset, while the bottom panel is for a dataset compiled by Hu et al. [9] but limited with MBD_{Rrs440} under 0.0005 sr^{-1} and in situ Chl under 1.0 mg/m^3. The fewer number of points for Chl_{OC4} of the NOMAD dataset is due to no R_{rs} measurements at 510 nm at some stations. The apparent plateau of Chl_{a440} is a result of the upper limit of MBD_{Rrs440} set as 0.0005 sr^{-1}.

the MBD_{Rrs}-a(440) scheme for *Chl* (Eqs. 1 to 2 and 4) was applied to monthly composites of SeaWiFS and MODIS (MODIS R_{rs}(547) was converted to R_{rs}(555) following the scheme developed by NASA; https://oceancolor.gsfc.nasa.gov/docs/ocssw/convert__band_8c_source.html), where the upper limit of MBD_{Rrs440} was extended to 0.0005 sr^{-1}. Figure 12A shows the histogram of Chl_{a440} obtained from SeaWiFS and MODIS, respectively, while Fig. 12B shows that of *Chl* obtained by the BGR_{Rrs} (OCx) algorithms. Clearly, as indicated in the study of Hu et al. [9], compared to the BGR_{Rrs} scheme, much better cross-sensor consistency was obtained from the MBD_{Rrs}-a(440) approach, further highlighting the advantages of the innovative band-difference scheme on estimating a(440) and *Chl*.

Table 2. Performance (in log10 scale) of 1- and 2-step empirical algorithms for the estimation of *Chl* from R_{rs}, for data with $MBD_{Rsrs440}$ less than 0.0005 sr^{-1} and in situ $Chl < 1.0$ mg/m^3. The fewer number of points for BGR_{Rrs} of NOMAD is due to no R_{rs} measurements at 510 nm at some stations.

	Algorithm	Slope	Intercept	R^2	RMSD	*N*
NOMAD	MBD_{Rrs}	0.88	−0.10	0.72	0.20	1,370
	BGR_{Rrs} (OC4)	0.77	−0.19	0.74	0.19	1,320
SeaWiFS-in situ	MBD_{Rrs}	0.84	−0.16	0.59	0.26	757
	BGR_{Rrs} (OC4)	0.66	−0.22	0.59	0.25	757

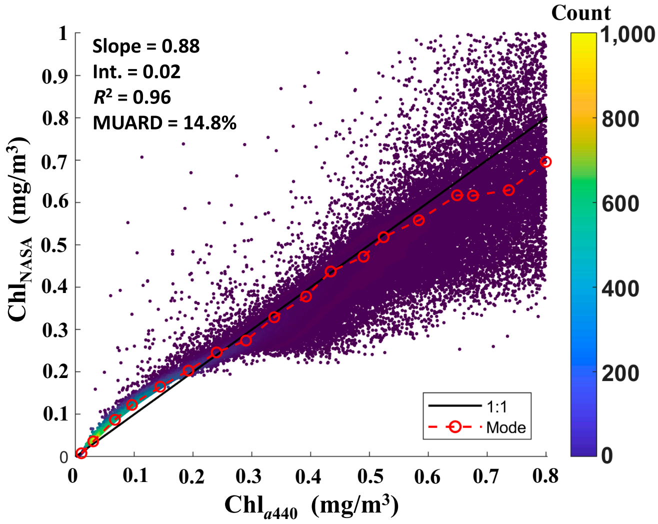

Fig. 10. Chl_{a440} compared with Chl_{NASA} for SeaWiFS measurements of 2010 November 14. The mode represents a common value of Chl_{NASA} for a given Chl_{a440}, which represents an average relationship between the 2 *Chl* products.

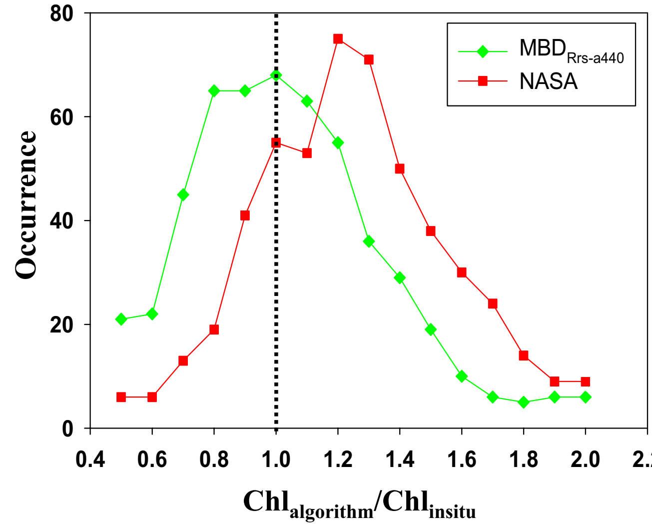

Fig. 11. Distribution of the ratio of *Chl* from algorithms to measured *Chl* for the NOMAD dataset with measured *Chl* < 0.15 mg/m^3 and MBD_{Rrs440} < −0.0005 sr^{-1}.

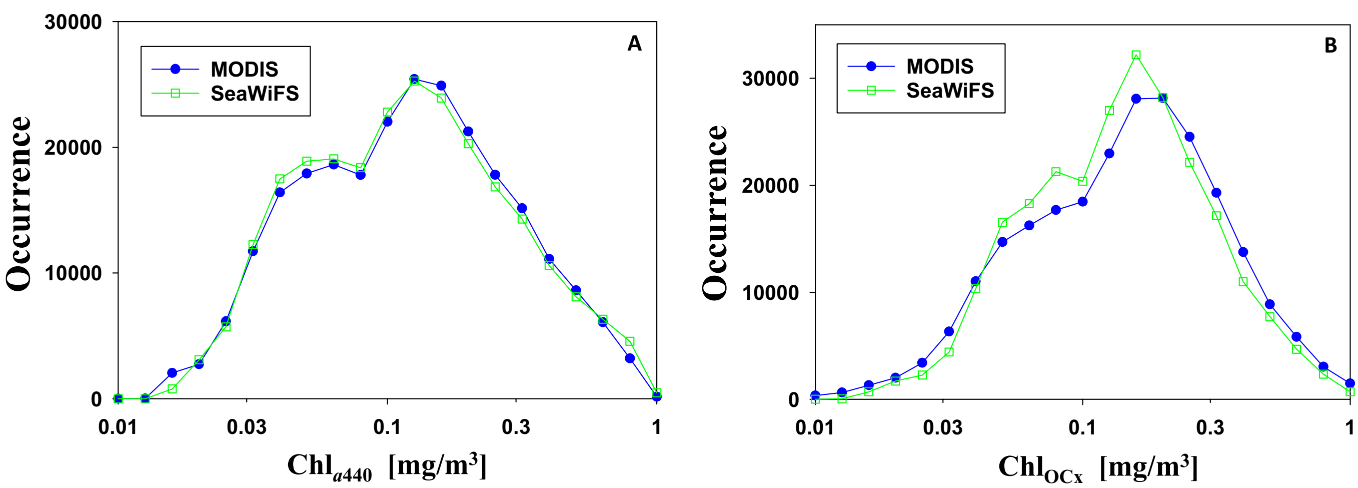

Fig. 12. Distribution of *Chl* obtained from MBD_{Rrs}-*a*(440) (A) and from BGR_{Rrs} (B), respectively, for measurements of SeaWiFS and MODIS during November 2006. The upper limit of MBD_{Rrs440} for the MBD_{Rrs}-*a*(440) approach is set as 0.0005 sr^{-1}.

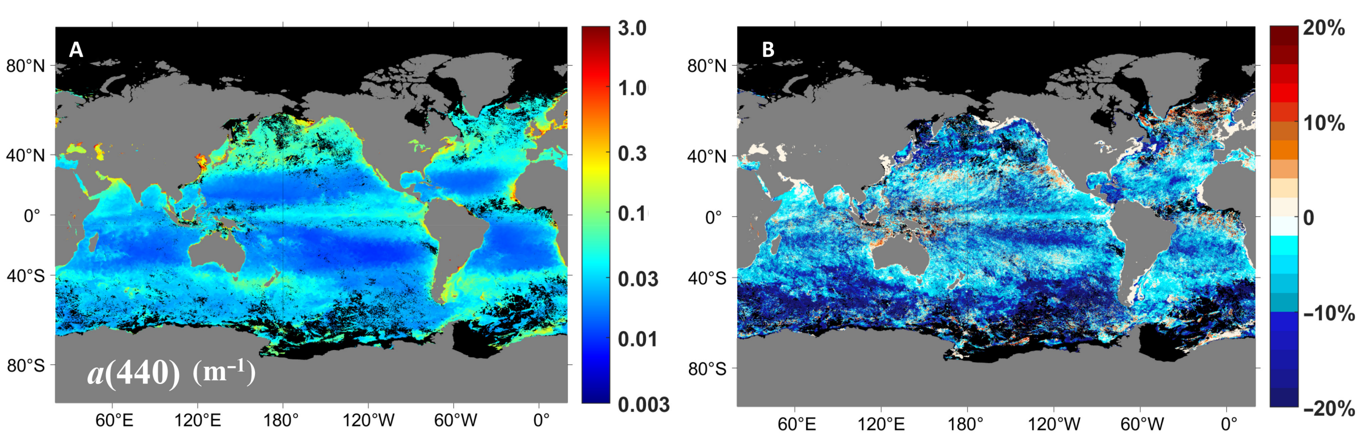

Fig. 13. (A) Global distribution of *a*(440) for SeaWiFS measurements of March 2006. (B) Relative difference between *a*(440) and $a(440)_{QAA}$ for data in (A).

D) Merge with *a*(440) from QAA for the global ocean

As MBD_{Rrs} works only for oligotrophic ocean, a merge with the absorption coefficient derived from other algorithms for less clear waters is necessary. The above analyses suggest that the MBD_{Rrs} scheme works well for MBD_{Rrs440} up to ~0.0005 sr^{-1}, with the equivalent $a(440)$ as 0.084 m^{-1}; thus, following Hu et al. [9], a merge was developed for the generation of $a(440)$ of the global ocean,

$$\begin{cases} a(440) = a(440)_{MBD};\ \text{if}\ \ MBD_{Rrs440} \le 0.0004\ \ sr^{-1}; & (6A) \\ a(440) = a(440)_{QAA};\ \text{if}\ \ MBD_{Rrs440} \ge 0.0005\ \ sr^{-1}; & (6B) \\ a(440) = \alpha \times a(440)_{MBD} + \beta \times a(440)_{QAA};\ \text{if}\ 0.0004\ \ sr^{-1} < MBD_{Rrs440} < 0.0005\ \ sr^{-1}; & (6C) \\ \alpha = \frac{0.0005 - MBD_{Rrs440}}{0.0005 - 0.0004}, \beta = 1 - \alpha & (6D) \end{cases}$$

Setting the upper limit as 0.0004 sr^{-1} for the derivation of $a(440)_{MBD}$ is a little more conservative but still covers $a(440)$ as high as 0.078 m^{-1} (equivalent *Chl* as ~0.7 mg/m^3). As an example, Fig. 13A shows the global distribution of $a(440)$ based on SeaWiFS monthly R_{rs} composite of March 2006, where the general patterns are consistent with our understandings of the spatial distribution of phytoplankton in the global oceans. Figure 13B shows the relative difference between $a(440)$ and $a(440)_{QAA}$ ($(a(440) - a(440)_{QAA})/a(440)_{QAA}$), which indicates that, in general, the two products are consistent for oligotrophic waters. The differences (most within ±10%), especially for the southern ocean, indicate the impact of noises in satellite R_{rs} on the estimation of $a(440)$ by such semianalytical algorithms, although algorithm approaches would also contribute to this difference (generally less than ~5%, see Fig. 2).

Conclusions

In the last decades, various algorithms have been developed for the estimation of *Chl* or IOPs from ocean color (R_{rs}), but only the algorithm based on multiband difference of R_{rs} (MBD_{Rrs}) developed for *Chl* shows strong tolerance to noises in R_{rs} for applications in oligotrophic waters. Here, we extended this scheme to the estimation of absorption coefficient of oceanic waters, which, not surprisingly, shows that $a(440)$ can be well estimated from MBD_{Rrs}, where the obtained $a(440)$ image product is much smoother than that obtained from a semianalytical algorithm. We further converted $a(440)$ to *Chl* based on the "Case-1" assumption and obtained in general consistent *Chl* product as that distributed by NASA from SeaWiFS measurements. More importantly, it appears that the upper limit of MBD_{Rrs440} of the MBD_{Rrs} scheme could be extended from the −0.0005 sr^{-1} set a decade ago to ~0.0005 sr^{-1}, which expands the coverage of oceanic waters from ~73% to ~91% for application of the MBD_{Rrs} scheme, although an optimized upper limit should be determined after analyzing large number of satellite images. On the other hand, it is found that there is a ~20% difference in the estimated *Chl* for oceanic gyres that was based on the same MBD_{Rrs440} but from different approaches (1 step and 2 steps). Such a difference suggests a strong necessity of more accurate measurements of *Chl* and R_{rs} in such waters, as it could significantly impact the studies on phytoplankton dynamics in these gyres.

Acknowledgments

The authors would like to thank NASA for the distribution of SeaWiFS and MODIS ocean color products and two anonymous reviewers for constructive comments and suggestions. **Funding**: Financial support by the National Natural Science Foundation of China (#41890803, #41830102, #41941008, and #42250710150) is greatly appreciated. **Author contributions**: C.H. helped in data analysis and revised the manuscript. Z.L. conceptualized the study and drafted and finalized the manuscript. J.L. helped in data analysis. S.S. revised the manuscript. D.W. helped in data analysis. L.Z. performed data analysis and algorithm evaluations. **Competing interests:** The authors declare that they have no known competing financial interests or personal relationships that could have appeared to influence the work reported in this paper.

Data Availability

Satellite and field-measured data used in this study can be found at the SeaWiFS Bio-optical Archive and Storage System (SeaBASS, https://seabass.gsfc.nasa.gov/).

References

1. Morel A, Prieur L. Analysis of variations in ocean color. *Limnol Oceanogr*. 1977;22(4):709–722.
2. Gordon HR. Can the Lambert-beer law be applied to the diffuse attenuation coefficient of ocean water? *Limnol Oceanogr*. 1989;34(8):1389–1409.
3. Lee ZP, Du KP, Arnone R. A model for the diffuse attenuation coefficient of downwelling irradiance. *J Geophys Res*. 2005;110(C2):C002573.
4. Zaneveld JRV, Kitchen JC, Pak H. The influence of optical water type on the heating rate of a constant depth mixed layer. *J Geophys Res*. 1981;86(C7):6426–6428.
5. Lee Z, Marra J, Perry MJ, Kahru M. Estimating oceanic primary productivity from ocean color remote sensing: A strategic assessment. *J Mar Syst*. 2015;149:50–59.
6. Gordon HR, Morel A. *Remote assessment of ocean color for interpretation of satellite visible imagery: A review*. New York (NY): Springer-Verlag; 1983.
7. Carder KL, Chen FR, Lee ZP, Hawes SK, Kamykowski D. Semianalytic moderate-resolution imaging spectrometer algorithms for chlorophyll-a and absorption with bio-optical domains based on nitrate-depletion temperatures. *J Geophys Res*. 1999;104(C3):5403–5421.
8. IOCCG. *Remote Sensing of Inherent Optical Properties: Fundamentals, Tests of Algorithms, and Applications*. In: Lee Z-P, editor, Reports of the International Ocean-Colour Coordinating Group No. 5; Dartmouth, Canada; 2006.
9. Hu C, Lee Z, Franz B. Chlorophyll a algorithms for oligotrophic oceans: A novel approach based on three-band reflectance difference. *J Geophys Res*. 2012;117(C1):C01011.
10. Hu C, Feng L, Lee Z. Uncertainties of SeaWiFS and MODIS remote sensing reflectance: Implications from clear water measurements. *Remote Sens Env*. 2013;133:168–182.
11. O'Reilly J, Maritorena S, Mitchell BG, Siegel D, Carder KL, Garver S, Kahru M, McClain C. Ocean color chlorophyll algorithms for SeaWiFS. *J Geophys Res*. 1998;103(C1): 24937–24953.
12. Lee ZP, Carder KL, Arnone R. Deriving inherent optical properties from water color: A multi-band quasi-analytical algorithm for optically deep waters. *Appl Opt*. 2002;41(27):5755–5772.

13. Werdell PJ, Franz BA, Bailey SW, Feldman GC, Boss E, Brando VE, Dowell M, Hirata T, Lavender SJ, Lee ZP, et al. Generalized Ocean color inversion model for retrieving marine inherent optical properties. *Appl Opt*. 2013;52(10):2019–2037.
14. Mitchell C, Hu C, Bowler B, Drapeau D, Balch WM. Estimating particulate inorganic carbon concentrations of the global ocean from ocean color measurements using a reflectance difference approach. *J Geophys Res Oceans*. 2017;122(11):8707–8720.
15. Le C, Zhou X, Hu C, Lee Z, Li L, Stramski D. A color-index-based empirical algorithm for determining particulate organic carbon concentration in the ocean from satellite observations. *J Geophys Res Oceans*. 2018;123(10):7407–7419.
16. Lin J, Lee Z-P, Ondrusek M, Liu X-H. Hyperspectral absorption and backscattering coefficients of bulk water retrieved from a combination of remote-sensing reflectance and attenuation coefficient. *Opt Exp*. 2018;26(2):A157–A177.
17. Claustre H, Sciandra A, Vaulot D. Introduction to the special section bio-optical and biogeochemical conditions in the south East Pacific in late 2004: The BIOSOPE program. *Biogeosciences*. 2008;5(3):679–691.
18. Morel A, Maritorena S. Bio-optical properties of oceanic waters: A reappraisal. *J Geophys Res*. 2001;106(C4):7163–7180.
19. Preisendorfer RW. *Hydrologic optics vol. 1: introduction*. Springfield (VA): National Technical Information Service, Office of Naval Research; 1976.
20. Morel A. Optical modeling of the upper ocean in relation to its biogenous matter content (case I waters). *J Geophys Res*. 1988;93(C9):10749–10768.
21. IOCCG. Remote Sensing of Ocean Colour in Coastal, and Other Optically-Complex, Waters. Reports of the International Ocean-Colour Coordinating GroupDartmouth, Canada; 2000.
22. Lee Z, Tang J. The two faces of “Case-1” water. *J Remote Sensing*. 2022;2022:Article 9767452.
23. Lee Z, Wei J, Voss K, Lewis M, Bricaud A, Huot Y. Hyperspectral absorption coefficient of “pure” seawater in the range of 350–550 nm inverted from remote sensing reflectance. *Appl Opt*. 2015;54(3):546–558.
24. Mobley CD. *Light and water: Eadiative transfer in natural waters*. New York (NY): Academic Press; 1994.
25. Bricaud A, Morel A, Babin M, Allali K, Claustre H. Variations of light absorption by suspended particles with chlorophyll a concentration in oceanic (case 1) waters: Analysis and implications for bio-optical models. *J Geophys Res*. 1998;103(C13):31033–31044.
26. Bricaud A, Babin M, Claustre H, Ras J, Tieche F. Light absorption properties and absorption budget of Southeast Pacific waters. *J Geophys Res Oceans*. 2010;115(C8):C08009.
27. Morel A. Are the empirical relationships describing the bio-optical properties of case 1 waters consistent and internally compatible? *J Geophys Res*. 2009;114(C1):C01016.
28. Werdell PJ, Bailey SW. An improved bio-optical data set for ocean color algorithm development and satellite data product validation. *Remote Sens Environ*. 2005;98(1):122–140.
29. Polovina J, Howell E, Abecassis M. Ocean’s least productive waters are expanding. *Geophys Res Lett*. 2008;35(3):1–5.
30. McClain CR, Signorini SR, Christian JR. Subtropical gyre variability observedby ocean-color satellittes. *Deep-Sea Res*. 2004;II(51):281–301.
31. Sathyendranath S, Brewin RJW, Brockmann C, Brotas V, Calton B, Chuprin A, Cipollini P, Couto AB, Dingle J, Doerffer R, et al. An ocean-colour time series for use in climate studies: The experience of the ocean-colour climate change initiative (OC-CCI). *Sensors*. 2019;19(19):Article 4285.